Pergamon

PII: S0038-092X(98)00074-7

Solar Energy Vol. 63, No. 4, pp. 199–216, 1998

0038-092X/98 $—see front matter

RECENT ADVANCES IN ELECTROCHROMICS FOR SMART WINDOWS APPLICATIONS

C. G. GRANQVIST,* A. AZENS,* A. HJELM‡,* L. KULLMAN,* G. A. NIKLASSON,* D. RÖNNOW§,* M. STRØMME MATTSSON,* M. VESZELEI* and G. VAIVARS**

* The Ångström Laboratory, Department of Materials Science, Uppsala University, P.O. Box 534, S-751 21 Uppsala, Sweden

** Institute of Solid State Physics, University of Latvia, LV-1063 Riga, Latvia

Received 3 June 1998; revised version accepted 29 June 1998

Abstract—Electrochromic smart windows are able to vary their throughput of radiant energy by low-voltage electrical pulses. This function is caused by reversible shuttling of electrons and charge balancing ions between an electrochromic thin film and a transparent counter electrode. The ion transport takes place via a solid electrolyte. Charge transport is evoked by a voltage applied between transparent electrical conductors surrounding the electrochromic film/electrolyte/counter electrode stack. This review summarizes recent progress concerning: (i) calculated optical properties of crystalline WO_3, (ii) electrochromic properties of heavily disordered W oxide and oxyfluoride films produced by reactive magnetron bias sputtering, (iii) novel transparent reactively sputter-deposited Zr–Ce oxide counter electrodes and (iv) a new proton-conducting antimonic-acid-based polymer electrolyte. Special in depth presentations are given on elastic light scattering from W-oxide-based films and of electronic band structure effects affecting opto–chronopotentiometry data in Zr–Ce oxide. The review also contains some new device data for an electrochromic smart window capable of very high optical transmittance.

1. INTRODUCTION

Smart windows are characterized by their ability to vary the throughput of radiant energy—visible light as well as solar radiation. This function is obtained by incorporating a chromogenic material in the window, in most cases in the form of a thin film having photochromic, thermochromic or electrochromic properties (Lampert and Granqvist, 1990). This survey describes recent progress in electrochromics, i.e. on devices whose optical properties can be modulated by low-voltage electrical pulses. For earlier work and background material, we refer to a number of recent books and review papers (Granqvist, 1993a, 1995, 1997; Agnihotry and Chandra, 1994; Bange *et al.*, 1995; Monk *et al.*, 1995; Lampert, 1998).

Figure 1 shows an electrochromic five-layer prototype device which introduces basic design concepts and types of materials. The central part of the construction is a purely ionic conductor (electrolyte), either a thin film or a polymeric laminate material; it must be a good conductor for small ions such as H^+ or Li^+. The electrolyte is in contact with an electrochromic layer and a counter electrode. The latter, in the case of a transparent device, must remain non-absorbing irrespective of its ionic content or exhibit electrochromism in a sense opposite to that of the base electrochromic film. Ideally, the electrochromic film (counter electrode) should display strong cathodic (anodic) electrochromism, or *vice versa*. This three-layer configuration is positioned between transparent electrical conductors.

By applying a voltage between the outer layers, ions can be shuttled into and out of the electrochromic film(s) whose optical properties are changed, thereby modifying the overall optical performance of the device. Physically, the optical modulation—at least in strongly disordered electrochromic films—is due to a variable polaron absorption associated with electrons introduced along with the ions.

Electrochromism can be used not only to regulate the throughput of radiant energy in a smart window, as implied above, but also for several other purposes. Section 2 outlines the most important of these and also surveys some critical materials issues. The most widely studied electrochromic film material is W oxide; recent work on this material is discussed in Section 3, specifically as regards computed optical properties of crystalline WO_3, and measured properties of heavily disordered W oxide (made with and

‡Present and permanent address: Helax AB, Box 1704, S-751 47 Uppsala, Sweden.

§Present and permanent address: ABIOF, Electrum 236, S-13440 Kista, Sweden.

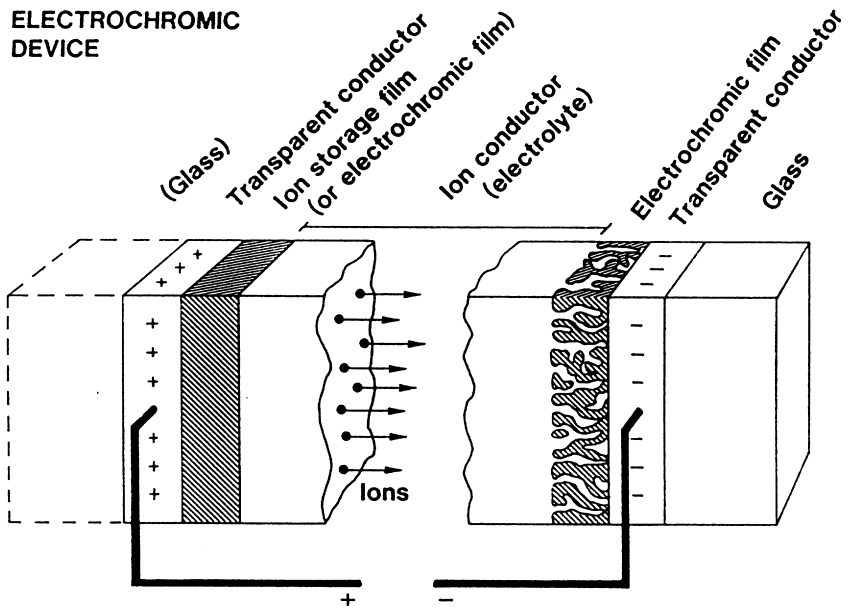

Fig. 1. Basic design of an electrochromic device, indicating transport of positive ions under the action of an electric field.

without electron bombardment) and W oxyfluoride. Section 4 treats novel data on Ce-containing counter electrodes capable of remaining fully transparent irrespective of their ionic content; the presentation is focused on Zr–Ce oxide films. Some results on an interesting new class of H^+ conducting adhesive electrolytes is reported on in Section 5. Finally, Section 6 gives some device data and a summary of the main results presented in this review.

2. ELECTROCHROMIC DEVICE TYPES, AND SURVEY OF MATERIALS OPTIONS

The smart window is only one of the interesting applications areas for electrochromism and not necessarily the one where electrochromism will first be introduced on a large scale. In fact, there are four different fields within which electrochromic devices offer distinct advantages over alternative technologies; they are schematically represented in Fig. 2. The smart window in Fig. 2(a) is readily understood from the discussion in Section 1. Such windows are likely to have important applications in innovative and energy-efficient architecture where they would adjust the inflow of luminous radiation and solar energy through glazings in buildings and large atria; the diffuse scattering (haze) can be practically nil. Smart windows may eventually have a profound influence on architecture and lead to new design philosophies with window apertures and wall claddings having regulatory functions, thus making buildings perform intelligently in concert with their ambience.

By replacing one of the transparent electrical conductors of the smart window with a specularly reflecting metallic reflector, one reaches the variable-reflectance device of Fig. 2(b). Its applications include anti-dazzling rear view mirrors for cars and trucks. If one integrates a white pigment in the electrochromic device, it can serve for information display purposes as depicted in Fig. 2(c). The black/white contrast and off-normal viewing properties can be excellent, holding promise for important applications in "signs" and "labels" of different kinds. Another possible device area concerns surfaces with variable thermal emittance, as sketched in Fig. 2(d); such surfaces are of interest for temperature stabilization of satellites.

There are many materials and design issues for practical electrochromic devices. Electrochromism is found in numerous organic and inorganic materials (mainly transition metal oxides). Figure 3 illustrates, by way of the periodic table, the metals known to produce cathodic and anodic electrochromic oxides. W oxide is the most widely studied electrochromic material (Granqvist, 1993a; Granqvist, 1995); it will be further discussed below. Ti oxide has recently been shown to exhibit very similar properties. Initial work (Gutarra *et al.*, 1994) used sputter deposition in a fluorine-containing plasma, but it has since become clear that favorable

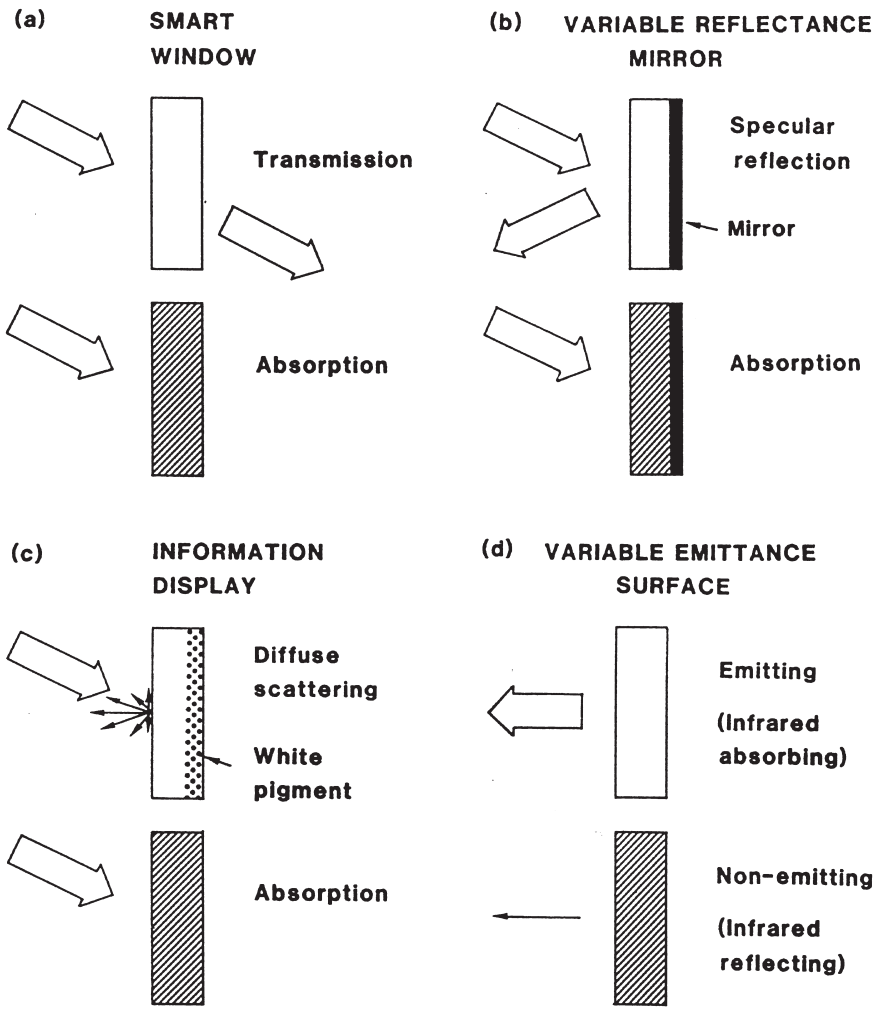

Fig. 2. The principles of four different applications of electrochromic devices. Arrows indicate incoming and outgoing electromagnetic radiation intensity.

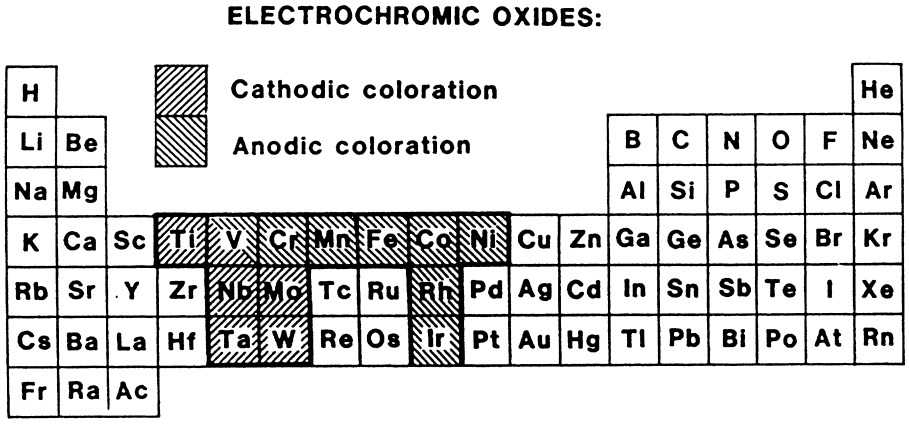

Fig. 3. The periodic table of the elements, excluding the lanthanides and actinides. The shaded boxes refer to the transition metals whose oxides have well-documented cathodic and anodic electrochromism.

electrochromic properties can be achieved under suitable conditions also in the absence of fluorine (Azens *et al.*, 1996; Kullman *et al.*, 1997). High-rate sputter deposition of certain electrochromic oxides is feasible by using plasmas containing CF_4, as reported in Section 3.2,

as well as by multi-cathode arrangements (Kharrazi *et al.*, 1997).

The counter electrode is a very important part of the electrochromic device, and—whereas research during the past 25 years has been focused on discovering electrochromic effects in thin films—the less spectacular but equally important task of finding suitable counter electrodes has received less attention. Generally speaking, five principle approaches have been used for the counter electrode: The first and most radical one does away with the counter electrode and employs one of the transparent electrical conductors as repository for the mobile ions when the electrochromic film is in its deintercalated state. Work on Li intercalation/deintercalation in films of crystalline doped In oxide and Sn oxide (Steele and Golden, 1991) has not given promising results, and a basic conflict between ion conduction requiring a porous structure and electrical conductivity requiring a dense structure seems to prevent substantial progress. The second approach relies on a non-solid electrolyte with dispersed redox couples; it has been used in prototype smart windows (Kamimori *et al.*, 1987), but the semi-solid character of the electrolyte should preclude large area applications. The third option uses a counter electrode that colors in the same manner as the electrochromic film though with a much lower efficiency. Crystalline WO_3 has this property (Cogan *et al.*, 1985) but its compact nature creates difficulties to accomplish rapid ion intercalation/deintercalation. The fourth, and in principle most elegant possibility, is to have a counter electrode that colors oppositely to the coloration of the electrochromic layer so that shuttling of ions between the two layers renders both of them either transparent or absorbing. This complementary design has been exploited for films of W oxide operating in conjunction with Ni oxyhydroxide (Svensson and Granqvist, 1986, 1987; Bange *et al.*, 1995), Ir oxide (Yamanaka, 1991; Rauh, 1995), $LiCoO_2$ (Goldner *et al.*, 1994) and $Fe_4^{3+}[Fe^{2+}(CN)_6]_3$ or $KFe^{3+}Fe^{2+}(CN)_6$ (known as Prussian Blue) (Ho *et al.*, 1994; Inaba *et al.*, 1995). Ni oxyhydroxide and Ir oxide have thus far been unambiguously documented only with proton intercalation/deintercalation, whereas Prussian Blue operates with K^+ intercalation/deintercalation. Li^+ transport is most popular for electrochromic devices; $LiCoO_2$ functions adequately in this case, but so far it has not been possible to obtain transparency over the full range of the luminous spectrum. A related, though somewhat more complicated counter electrode, is V_2O_5 which shows complementarity to W oxide at short wavelengths (Talledo and Granqvist, 1995). The latter material has been used in several devices (Andersson *et al.*, 1989; Baudry *et al.*, 1991; Ashrit *et al.*, 1993; Zhang *et al.*, 1994), and possibilities to improve the V oxide by Cr or Nb addition (Cogan *et al.*, 1993) and fluorination (Talledo *et al.*, 1994) have been explored. The fifth type of counter electrode, considered in some detail below, is the one that remains fully transparent irrespective of its ionic content. These properties have been achieved in films containing CeO_2, as further discussed in Section 4. Among the remaining possibilities to obtain counter electrodes, one may notice catalytically active Au films (Deb and Witzke, 1975; Svensson and Granqvist, 1985; Deb, 1992, 1995) whose inherent absorption, however, limits the overall transparency to $\sim 50\%$, and certain polymeric layers (Lampert *et al.*, 1994; Tassi and de Paoli, 1994). The references to work on the different types of counter electrodes are by no means complete, and a more detailed listing is found in the work by Kullman *et al.* (1997).

The centrally positioned ion conductor can be of several kinds. Hydrous oxidic thin films can serve as H^+ conductors, and H^+ conduction is possible also in polymeric materials, as touched upon in Section 5. Certain polymers containing Li perchlorate, Li triflate, etc. may be very well suited to large area devices such as smart windows; Azens *et al.* (1992) report on a Li^+ conducting polymer that has given promising results in recent device-oriented work. It is not enough that the polymer electrolyte exhibits a high ion conductivity, but adhesiveness to the pertinent electrochromic film and counter electrode is necessary to avoid delamination and achieve a sufficient device lifetime.

The final device components are the transparent electrical conductors (Granqvist, 1993b), with In_2O_3:Sn (often referred to as ITO) having the best electrical properties. The conductivity is produced by Sn atoms substituting In in the lattice, thereby providing n-doping by one electron per Sn as long as the tin atoms are sufficiently dispersed to avoid significant clustering (Hamberg and Granqvist, 1986). From a practical point of view, the availability and cost of In may be problematic, and it would be desirable to decrease the amount of this metal. Work on ternary compounds such as

$Zn_2In_2O_5$ (Enoki *et al.*, 1992), $GaInO_3$ (Cava *et al.*, 1994; Phillips *et al.*, 1994), $MgIn_2O_4$ (Ueda *et al.*, 1992; Un'no *et al.*, 1993), $ZnSnO_3$ (Minami *et al.*, 1994), Zn_2SnO_4 (Minami *et al.*, 1995a), as well as $MgO–In_2O_3$ and $ZnO–In_2O_3$ (Minami *et al.*, 1994, 1995a,b, 1996a,b) is interesting in this regard, and all of these compounds are capable of producing transparent electrical conductors.

3. ELECTROCHROMISM IN W OXIDE

3.1. Electronic structure and calculated optical properties of crystalline WO_3

It was noted above that W oxide is the most widely studied electrochromic material. Bearing this in mind, we considered it worthwhile to carry out a detailed study of the electronic structure and optical properties of crystalline WO_3 (Hjelm *et al.*, 1996). It should be remembered, though, that most practically useful W oxide films are heavily disordered, implying that the results described below cannot be directly transformed into predictions for electrochromic films. In particular, the crystalline WO_3 can attain high infrared reflectivity as a result of free electrons, whereas the disordered material instead absorbs in the near-infrared due to polarons (Granqvist, 1995).

Our calculations relied on the local approximation to density functional theory and used a full-potential linear muffin-tin orbitals method; details are given elsewhere (Hjelm *et al.*, 1996). A cubic (perovskite) structure was assumed in order to bring computation times within reasonable limits, and it was verified that an experimentally more plausible (Granqvist, 1995) hexagonal crystalline modification does not lead to large changes. The reasons for this relative insensitivity to the details of the crystalline structure are that the relevant atomic displacements are small, and that the existence of WO_6 structural units has a dominating influence on the electronic structure.

Figure 4 displays a set of density of states (DOSs) curves, including projected DOSs. Part (a) shows that WO_3 behaves like a semiconductor with a valence band dominated by O p states and a conduction band dominated by W d states; there is considerable hybridization between these bands. The calculated bandgap is much smaller than the experimental one, which points at a common failure of the local density approximation applied to semiconducting systems. Figure 4(b) refers to $LiWO_3$, with the Li atom placed in the center of the perovskite unit cell. The overall features of the band structure remain unchanged, and the Li projected states appear high up in the conduction

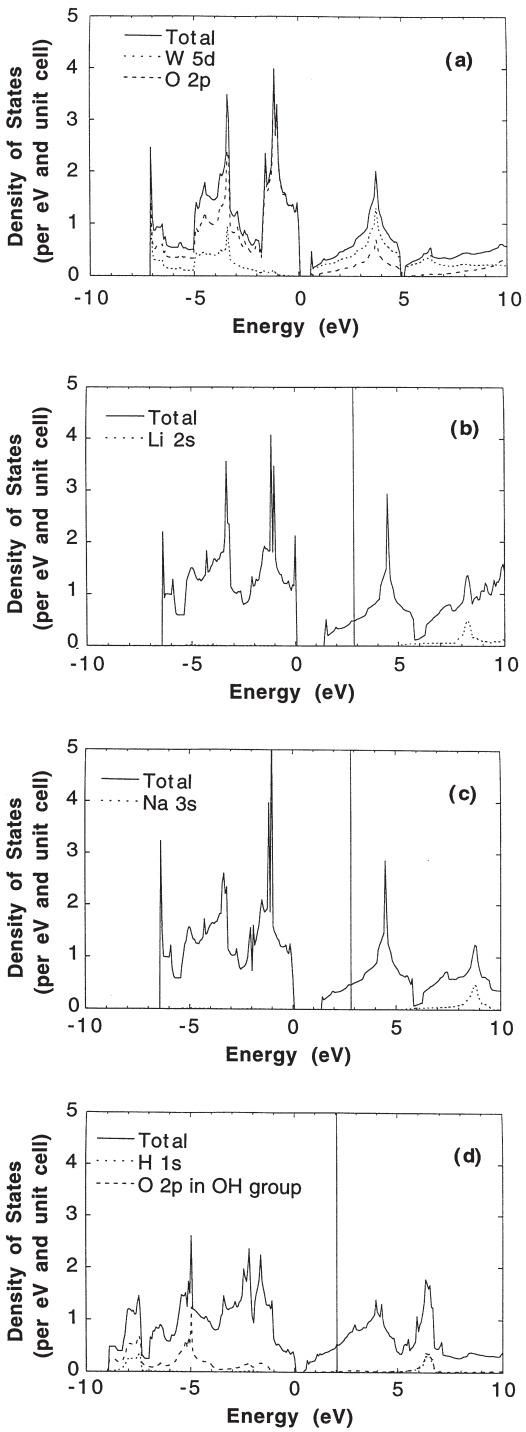

Fig. 4. Density of states for cubic (a) WO_3, (b) $LiWO_3$, (c) $NaWO_3$ and (d) HWO_3; the OH separation was 0.103 nm. Projected state densities are shown. Fermi energies are marked as vertical lines (for WO_3 the Fermi energy lies in the bandgap).

band, so that the Li essentially remains ionized. The associated electrons occupy states at the bottom of the conduction band, and the material is expected to be metallic with W d bands at the Fermi level. Figure 4(c) indicates that the DOS remains about the same for $NaWO_3$ as for $LiWO_3$. HWO_3 is not identical, though, and the hydrogen atom has to be displaced from the center of the perovskite unit cell in order to have minimum total energy. Detailed computations showed that the hydrogen atom should be positioned 0.103 nm from an oxygen atom, implying the formation of a hydroxyl unit. Figure 4(d) displays the DOS for HWO_3 with this structure. The similarity to the cases of $LiWO_3$ and $NaWO_3$ is apparent, and hence all of these materials are expected to have related properties. The applicability of a rigid band picture for the electronic structure is clearly seen from Fig. 4.

Optical properties were calculated essentially by obtaining the interband part of the dielectric function through a summation of transitions from occupied to unoccupied states (with constant wavevector) over the Brillouin zone, weighted with the matrix element giving the probability for the transition. The intraband contribution was represented by a Drude model. Figure 5 shows calculated spectral reflectance for Li_xWO_3 and Na_xWO_3, together with selected experimental results (see Hjelm *et al.* (1996) for details). The three sets of data are in good qualitative correspondence. The agreement could be improved by superimposing contributions due to polaron absorption.

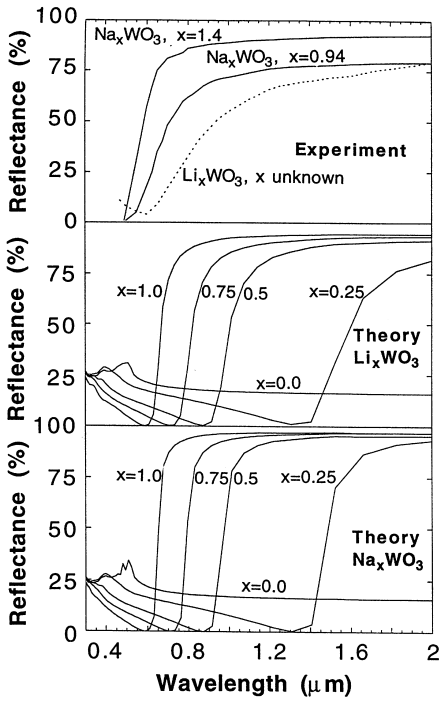

Fig. 5. Spectral reflectance for Li_xWO_3 and Na_xWO_3, illustrating experimental as well as computed results; cf. Hjelm *et al.* (1996) for details.

3.2. Preparation, characterization, electrochemical properties and specular optical data on fluorinated and electron-bombarded films

Recent work by Azens *et al.* (1995) showed that sputtering of tungsten in the presence of O_2+CF_4 could produce films with excellent electrochromism and a potential for reaching very high deposition rates by target heating promoting chemical effects. A drawback was that the fluorination impaired the durability under ion intercalation/deintercalation. The studies reported on below demonstrate, among other things, that electron (e) bombardment can enhance the durability considerably.

W-oxide-based films were produced by reactive DC magnetron sputtering in a gas mixture containing Ar, O_2, and, in many cases, CF_4. Films were formed on unheated glass substrates precoated with transparent and conducting layers of ITO. Detailed deposition conditions were given elsewhere (Azens *et al.*, 1995). The role of a bias voltage U_{bias} applied to the substrate was investigated in some detail. Oxide films with good electrochromic properties were produced at a deposition rate r of ~ 0.5 nm s^{-1} for 25 V $< U_{bias} <$ 80 V. These conditions correspond to a bombardment of 1 to 10 electrons per incident atom forming the film. Oxyfluoride films, on the other hand, had $r \sim 1.2$ nm s^{-1} for $U_{bias} < 0$ and low deposition rates for $U_{bias} > 50$ V. Most likely, the relation between r and U_{bias} for the oxyfluoride films depends on electron bombardment making the film surface very active for reactions with F-containing radicals, thus leading to volatile etch products.

Atomic force microscopy (AFM) was used to investigate surface topographies of ~ 0.6-μm-thick films produced under different conditions. Oxide films made in $Ar+O_2$ showed surface roughness with an average distance of ~ 0.1 μm between the protrusions; these features are believed to mirror a columnar microstructure of the film. A similar surface topography was found in oxyfluoride films made in $Ar+O_2+CF_4$. Electron bombardment through the application of a positive substrate bias of 70 V had a more drastic influence on the roughness, and AFM data indicated a column size of ~ 0.5 μm. One should notice that the effect of

the electron bombardment is opposite to that expected for ion bombardment, which is generally known to disrupt the columnar structure thereby giving rise to denser and smoother films (Johnson, 1991).

X-ray diffraction studies were made on films similar to those mentioned above and also on crystalline W oxide films that had undergone annealing in vacuum for 2 h at 420°C. Diffractograms for the e-bombarded and annealed samples showed clear features due to long-range lattice order, whereas no such features were apparent for the as-deposited oxide and oxyfluoride samples. The diffraction peaks were in principle in agreement with those found earlier in crystalline W oxide films made by several different techniques (Granqvist, 1995).

Infrared spectrophotometry was applied to the four types of films discussed above. The absorptance spectrum for the as-prepared W oxide film had a dominating peak at a wavenumber of $\sim 600\ cm^{-1}$, which is characteristic for the vibrational properties of a disordered tungsten–oxygen framework (Taylor and Patterson, 1994; Granqvist, 1995). The annealed and crystalline counterpart had absorption peaks at ~ 700 and $\sim 800\ cm^{-1}$, in good agreement with the phonon spectrum in WO_3 crystals. An e-bombarded film prepared with $U_{bias} = 35$ V showed an interesting absorption spectrum with unmistakable features of *both* the highly disordered and the crystalline states. The oxyfluoride film, finally, displayed a very broad absorption structure between 600 and $1000\ cm^{-1}$.

Raman spectrometry, yielding complementary information on the vibrational properties, was applied to ~ 0.7-μm-thick films. An as-prepared W oxide film had a broad peak at $\sim 780\ cm^{-1}$, characteristic of the W–O stretching modes in a disordered material (Shigesato *et al.*, 1991; Granqvist, 1995). Crystallization of such a sample made this feature split into two separate peaks, the one at $\sim 950\ cm^{-1}$ being caused by asymmetric stretching vibrations of W=O bonds mainly on internal surfaces. An oxide film grown under electron bombardment at $U_{bias} = 70$ V maintained the broad peak at $\sim 780\ cm^{-1}$—i.e. crystallization was not apparent—whereas the influence of the W=O bonds was clearly augmented. The latter effect is both interesting and unexpected, since even a partial crystallization ought to have diminished the W=O feature, and since the AFM data referred to above pointed at grain growth under electron bombardment and hence a decrease of any internal surface. An oxyfluoride film, finally, had less pronounced features due to W=O bonds.

Cyclic voltammetry was used to study various W-oxide-based films immersed in an electrolyte of propylene carbonate with 1M $LiClO_4$. A standard three-electrode arrangement was adopted with Li foil serving as counter electrode and reference electrode. Data were taken in a glove box under essentially water-free conditions. Some durability tests on electron-bombarded films were also carried out in a more aggressive electrolyte of 0.1M H_2SO_4.

Figure 6 shows cyclic voltammograms for Li intercalation/deintercalation in 0.6 to 0.7-μm-thick films. Part (a) refers to an oxyfluoride film and shows that the initial charge capacity is large. However, the voltammograms evolve during the cycling, and the charge capacity has decreased very much after 10^3 cycles. The change is more rapid than for typical W oxide films. The oxyfluoride still can be used after $\sim 10^4$ cycles, but significant ion intercalation/deintercalation can be maintained only by increasing the limits of the potential sweep.

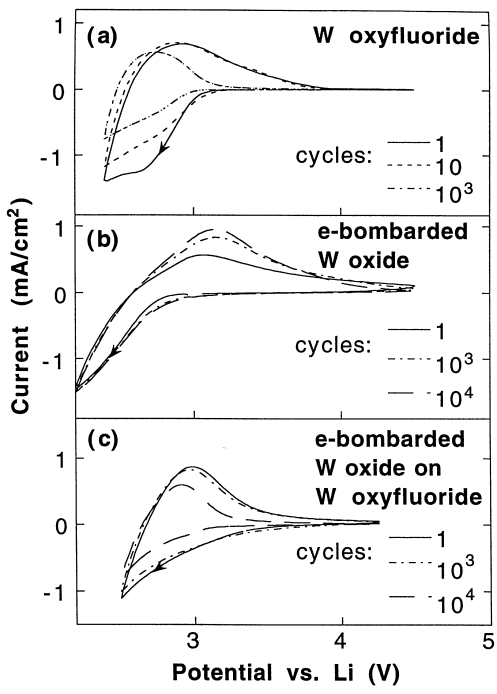

Fig. 6. Cyclic voltammograms for (a) a W oxyfluoride film, (b) a W oxide film prepared under electron bombardment with $U_{bias} = 22$ V and (c) a tandem with a W oxyfluoride film covered with a thin layer of e-bombarded W oxide. Data are given for different numbers of voltammetric cycles. The voltage scan rate was $50\ mV\ s^{-1}$. Arrows indicate scan direction.

Figure 6(b) reports data for an e-bombarded W oxide film produced with $U_{bias} = 22$ V. The voltammogram is very different from that of the oxyfluoride, and the charge capacity does not show any signs of decline even after 10^4 cycles. The main cycle-dependent evolution takes place in the part of the voltammogram that corresponds to Li^+ deintercalation. A charge imbalance for the intercalation/deintercalation reaction was found during the initial cycling, whereas the inserted and extracted charge remained stable at 15.1 mC cm^{-2} after 10^4 cycles between 2.5 and 4.5 V versus Li.

Particularly interesting results were obtained with a tandem film having a 0.6-μm-thick W oxyfluoride layer covered with a 0.05-μm-thick protective film of e-bombarded W oxide made with $U_{bias} = 22$ V. The voltammogram in Fig. 6(c) shows that the tandem combines the assets of the constituent layers, viz. the large charge capacity of the oxyfluoride and the good durability of the e-bombarded oxide. The overall shape of the voltammogram is similar to that of heavily disordered W oxide (Granqvist, 1995). It is noteworthy that the top layer does not prevent the Li^+ ions from penetrating easily into the underlying film. We also tested a 0.7-μm-thick film of e-bombarded W oxide in 0.1M H_2SO_4 under potentiostatic switching between $+1$ and -1 V versus Ag/AgCl at 0.2 Hz. The film remained functional as an intercalation/deintercalation host even after 10^5 cycles, which points at a remarkable durability.

Spectral optical transmittance was measured in the $300\ \text{nm} < \lambda < 2500$ nm wavelength range by spectrophotometry. Figure 7 shows data for a $\sim$0.6-μm-thick film of e-bombarded W oxide prepared with $U_{bias} = 35$ V; the colored and bleached states were obtained by applying 2.3 and 4.3 V versus Li, respectively, for 100 s. The range of optical modulation is large, and the luminous transmittance was 74% for the bleached state and 3% for the colored state. The coloration efficiency was 30 to 40 cm^2 C^{-1} at $\lambda = 550$ nm for e-bombarded W oxide films and $\sim$60 cm^2 C^{-1} for oxyfluoride films. Literature data for typical W oxide films lie at 40 to 50 cm^2 C^{-1} at $\lambda = 550$ nm (Granqvist, 1995).

The color/bleach dynamics is critically dependent on the technique for making the film, as can be understood from voltammetry data. Figure 8 reports transmittance at $\lambda = 550$ nm when the films earlier reported on in Fig. 6 were subjected to 2.3 V versus Li for 50 s followed by 4.3 V versus Li for another 50 s. The W oxyfluoride film was in virgin state, while the other films had undergone 5000 voltammetric cycles.

The dynamics of the single e-bombarded oxide and oxyfluoride films are remarkably different, with the latter being capable of going from 75% to 10% in 5 s and returning from a low to a high transmittance in a comparable time span. The tandem film has a similar dynamics, though it does not attain as low a transmittance as the oxyfluoride. Figure 8 is a striking illustration of the good properties obtainable in tandem films. It is possible that the top layer prevents dissolved oxyfluoride species from leaving the film, in analogy with the effect that polymeric Nafion layers can have on W oxide films (Shen *et al.*, 1992). The slow response of the e-bombarded W oxide films can be partly alleviated if they are used in an electrolyte of 0.1M H_2SO_4. It was then possible to reach a transmittance below a few percent

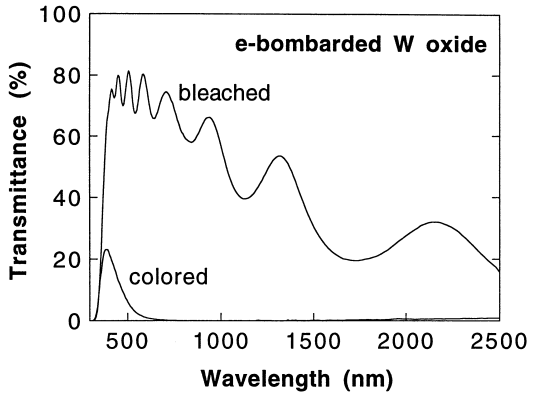

Fig. 7. Spectral transmittance for an e-bombarded W oxide film prepared at $U_{bias} = 35$ V. The curves refer to the sample in colored and bleached states.

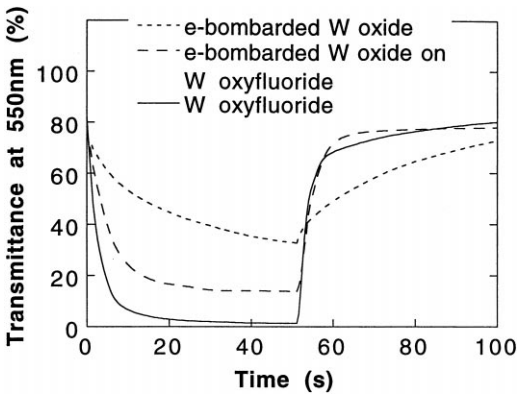

Fig. 8. Transmittance at $\lambda = 550$ nm during coloration and bleaching of the shown types of films, produced as described in Fig. 6.

under experimental conditions analogous to those underlying Fig. 8.

3.3. Special feature: elastic light scattering and electrochemical durability

Practical fenestration must avoid perceivable haze. Having this in mind, a detailed study was carried out on electrochromic W oxide films, deposited as described in Section 3.2 onto transparent substrates (Kullman *et al.*, 1996; Rönnow *et al.*, 1996). A complementary investigation considered analogous films backed by metallic reflecting substrates (Lindström *et al.*, 1997).

Total and diffuse transmittance (T_t and T_d, respectively) were studied as a function of wavelength using a total integrated scattering instrument whose main features are shown in Fig. 9. Diffusely transmitted light is focused onto the detector by a spherical mirror, while the directly transmitted light goes through an aperture into a beam dump. Total transmittance is obtained by putting a plug in the aperture. A detailed description of this newly developed equipment is given elsewhere (Rönnow and Veszelei, 1994). Spectra were recorded at 400 nm $< \lambda <$ 1000 nm for the three types of film in their as-deposited (ad) state and after 10, 100 and 1000 voltammetric cycles. Prior to the optical measurements, the samples were removed from the electrolyte, washed in ethanol and purified water, and blown dry with nitrogen gas.

Figure 10 shows $T_t^\gamma(\lambda)$ and $T_d^\gamma(\lambda)$ (where the superscript γ stands for ad, 10, 100 and 1000, and hence refers to the sample treatment). The electrochromic films were in their fully bleached states. $T_t^\gamma(\lambda)$ is close to unity for all samples, irrespective of treatment, with the exception of a decrease at $\lambda < 450$ nm for the e-bombarded W oxide.

The magnitudes of $T_d^\gamma(\lambda)$ are different for the three samples. Figure 10(a), pertaining to "standard" W oxide, shows that T_d^γ is as low as 3.5 to 9×10^{-4} at $\lambda = 400$ nm, and this quantity decreases with increasing wavelength so that even lower values (down to 1 to 2×10^{-4}) are found at $\lambda = 900$ nm. The W oxyfluoride film, reported on in Fig. 10(b), has a weaker spectral dependence of T_d^γ with magnitudes lying between 1×10^{-3} and 3×10^{-3}. The e-bombarded W oxide sample in Fig. 10(c) shows a qualitatively different performance, with T_d^γ approaching 10^{-1} at $\lambda = 450$ nm. The

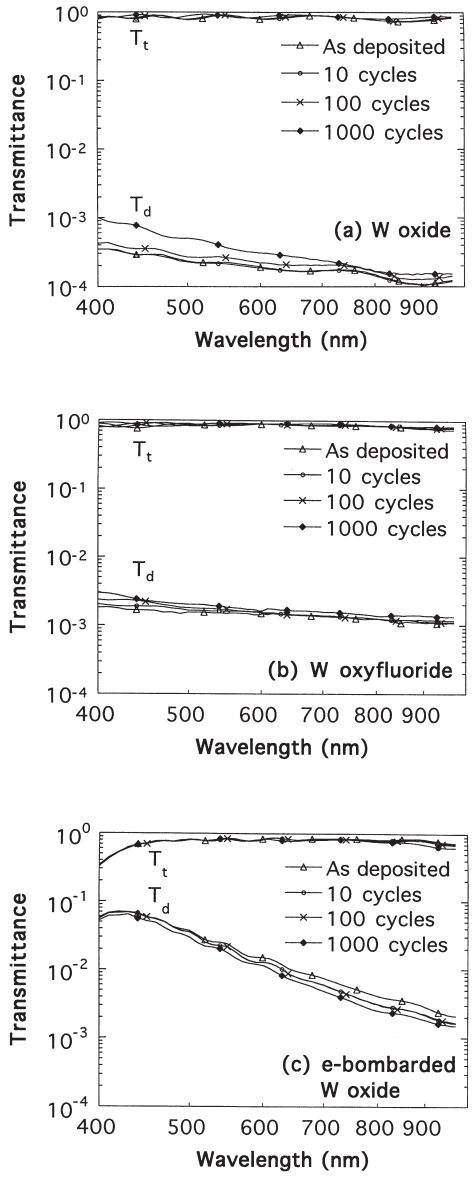

Fig. 10. Spectral total and diffuse transmittance (T_t and T_d, respectively) for films in the as-deposited state and after voltammetric cycling. Parts (a), (b) and (c) refer to W oxide, W oxyfluoride and e-bombarded W oxide prepared with $U_{bias} = 120$ V, respectively.

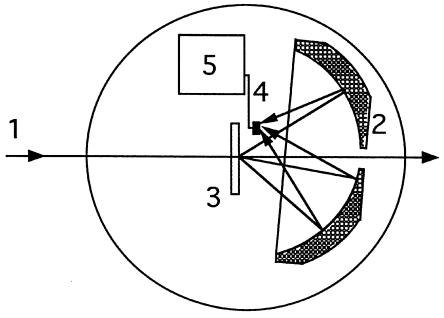

Fig. 9. Outline of the total integrating scattering instrument arranged for diffuse scattering measurement, showing incident beam (1), focusing mirror (2), sample (3), detector (4) and preamplifier (5).

scattering falls off rapidly with increasing wavelength, and is as small as 1 to 2×10^{-3} at $\lambda=$ 900 nm. The data for T_d^{ad}, T_d^{10}, T_d^{100} and T_d^{1000} are not significantly different, and hence the degradation observed for W oxide and oxyfluoride does not lead to a change in scattering. The largest effect was observed in T_d^{1000} for W oxide (cf. Figure 10(a)), but similar differences could be observed for measurements at different parts of the sample so that this effect cannot be taken to be significant.

The diffuse and total transmittance of rough surfaces can be related to each other through different theories. Scalar scattering theory gives $T_d = T_t[2\pi(1-n)(\delta/\lambda)]^2$, where n is the refractive index and δ is the root-mean-square (RMS) roughness (Carniglia, 1979). The data in Fig. 10 can be interpreted in terms of a surface roughness that, quantitatively, is as low as a few nanometers for W oxide and W oxyfluoride and about an order of magnitude larger for e-bombarded W oxide. As pointed out above, AFM profiles revealed that e-bombarded W oxide has larger grains than W oxide and W oxyfluoride, and is rougher on lateral length scales of the order of the wavelength of light and longer; this is in qualitative agreement with empirical results.

A rule-of-thumb states that haze becomes visible when T_d is $\sim10^{-2}$. Hence the e-bombarded film is non-ideal, whereas both the conventionally prepared W oxide film and the W oxyfluoride film have a clear appearance. It is noteworthy that the roughness does not seem to increase during the degradation. It should also be remarked that the simplistic scalar theory underlying the formula for T_d above can be replaced by an elaborate vector perturbation theory applicable to multilayers with rough interfaces (Duparré, 1995) and volume inhomogeneities (Amra, 1993). Vector perturbation theory was used recently to investigate the elastic light scattering of W oxide films on transparent and reflecting substrates, and features of scattering spectra for both colored and bleached samples could be modeled (Kullman *et al.*, 1996a; Rönnow *et al.*, 1996; Lindström *et al.*, 1997).

4. TRANSPARENT COUNTER ELECTRODES BASED ON Ce OXIDE

4.1. Preparation, characterization, electrochemical properties and optical data

It has been known for some time that films of Ti–Ce oxide can combine optical transparency with an ability to insert/extract large charge densities so that such films are of interest as counter electrodes in smart windows (Gomes *et al.*, 1992; Lavrencic Stangar *et al.*, 1993; Kéomany *et al.*, 1994, 1995; Camino *et al.*, 1995; Kullman *et al.*, 1997; Strømme Mattsson *et al.*, 1997). Below we report on recent work showing that Zr–Ce oxide films have superior properties and can be almost fully transparent over the entire visible spectrum under the charge exchange of as much as 0.5 Li^+ ions per Ce atom (Veszelei *et al.*, 1997, 1998).

Films of pure ZrO_2, CeO_2 and mixed Zr–Ce oxide were prepared by reactive DC magnetron sputtering in an atmosphere of $Ar+O_2$ so that the O_2/Ar gas flow ratio was in the 0.02–0.1 interval. Detailed deposition conditions are given by Veszelei *et al.* (1998). Glass substrates precoated with ITO were used in most cases.

Elemental compositions were determined by Rutherford backscattering spectrometry (RBS). It was found that the elemental compositions of all of the mixed films could be expressed as $Zr_zCe_{1-z}O_{2+\delta}$ with δ ranging up to 0.6. The oxygen surplus—i.e. the fact that δ is larger than zero—is most likely associated with adsorbed water. This surmise is supported by infrared reflectance data described below. Structural characterization was performed by X-ray diffraction (XRD). Most of the films were found to be polycrystalline, which can be contrasted with earlier work on Ti–Ce oxide in which the sputtered films were amorphous (Kullman *et al.*, 1997; Strømme Mattsson *et al.*, 1997). Mixed oxide films exhibited cubic structures when the Ce content was high enough. It may be noted that ZrO_2 can have one of three crystal structures: monoclinic, tetragonal or cubic, with the latter two being high-temperature phases. The XRD peaks were consistent with literature data but were too broad to resolve details of the structure. Considering the widths of the XRD peaks, the crystal sizes were found to be about 7 nm. A cubic lattice parameter was calculated from XRD using the (111), (002) and (022) reflections. The data lay on a straight line coinciding with the lattice parameters for bulk $Zr_{0.4}Ce_{0.6}O_2$, $Zr_{0.25}Ce_{0.75}O_2$ and CeO_2. Furthermore, the data were in agreement with an empirical relation (Kim, 1989) to account for the lattice parameter of fluorite-structure CeO_2 with ZrO_2 added as a solid solution.

Infrared absorption spectroscopy was used in order to obtain complementary structural infor-

mation, specifically using the reflectance of p-polarized light impinging at an off-normal angle of 60° in the 200 to 5000 cm^{-1} wavenumber interval. All of the films displayed a broad absorption band centered around a wavenumber of 3400 cm^{-1}, which corresponds to the OH^- stretching region and points at the hydrous nature of the films. The region 1200–1700 cm^{-1} contained a few weaker absorption peaks. Spectral reflectance measured between 350 and 1200 cm^{-1} displayed one major absorption peak around 600 cm^{-1} for each film of the mixed oxides, near the longitudinal optical (LO) phonon of bulk CeO_2 (Mochizuki, 1982). This peak is only noted in the reflectance of p-polarized light, which verifies its LO character. The position of this absorption peak shifted towards higher energies when the Ce content was decreased; a similar tendency has been noted for Ti–Ce oxides (Kullman *et al.*, 1997).

Films deposited onto ITO-coated glass were immersed in an electrolyte of propylene carbonate with 1M $LiClO_4$. They were studied by cyclic voltammetry in order to get an overall picture of the charge insertion/extraction processes. More quantitative results, obtained by chronopotentiometry, are discussed shortly in Section 4.2. The measurements were performed in a three-electrode configuration with the film under study as working electrode and Li foil serving as counter electrode and reference electrode. Figure 11 shows cyclic voltammograms for ZrO_2, CeO_2 and Zr–Ce oxide with the shown compositions. The ZrO_2 film is practically incapable of charge insertion/extraction. The charge capacity for the mixed oxide films increases with Ce content. Pure CeO_2 is able to sustain a large charge exchange, but these films degraded seriously; the charge capacity decreased from 61 to 3 mC cm^{-2} μm^{-1} during 400 cycles. The data in Fig. 11 were taken after a few cycles, i.e. before major degradation had begun. Figure 12 reports quantitative data on the inserted and extracted charge densities—denoted Q_i and Q_e, respectively—during voltammetric cycling of Zr–Ce oxide films between the endpoints illustrated in Fig. 11 with a voltage sweep rate of 50 mV s^{-1}. The data exhibit a complex behavior when the number of cycles is below ~100. After some 1000 cycles, though, the magnitudes of Q_i and Q_e stabilize at about 13 mC cm^{-2} μm^{-1}; this value pertains to the film with the highest Ce content. It is interesting and technically important to note that mixed

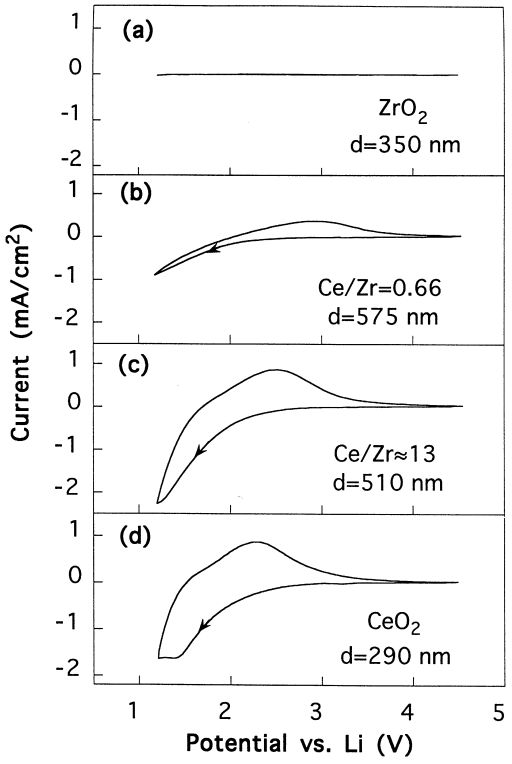

Fig. 11. Cyclic voltammograms of sputter-deposited Zr–Ce oxide films with different compositions, together with data for pure Zr and Ce oxide. The voltage sweep rate was 50 mV s^{-1}. Arrows denote sweep direction. The film thickness d is indicated.

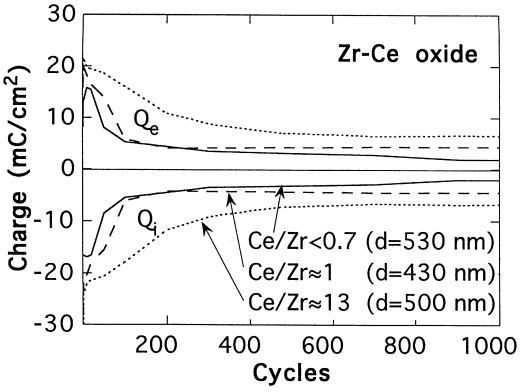

Fig. 12. Charge density for sputter-deposited Zr–Ce oxide films with different compositions and thickness d. The films were cycled between the potentials 1.2 and 4.5 V versus Li. Inserted and extracted charge densities are denoted Q_i and Q_e, respectively.

Ce-oxide-based films are more stable than pure Ce oxide and able to yield reversible charge insertion/extraction for a large number of cycles.

Optical measurements were performed in the 300 nm $< \lambda <$ 2500 nm range by use of a spectrophotometer with an integrating sphere. *In situ* data were taken with the film/substrate tandem

in a cell, containing electrolyte and Li foil electrodes, mounted in the sample compartment of the instrument. The cell was equipped with polished quartz windows; it was sealed inside a glovebox prior to the measurements. Figure 13 shows transmittance in the 300 nm $< \lambda <$ 850 nm interval for a Zr–Ce oxide film exhibiting a high transmittance over the full visible spectrum (400 nm $< \lambda <$ 700 nm). It is interesting to observe that electrochemical cycling, performed in the same way as for recording the cyclic voltammograms, led to improved transmittance in the ultraviolet. The same effect has also been noted for oxides of Ti–Ce, W–Ce and Sn–Ce (Kullman *et al.*, 1996b).

Transmittance changes during charge insertion/extraction were recorded at $\lambda = 550$ nm under Li^+ intercalation at 1.2 V versus Li for 20 s followed by deintercalation at 4.5 V versus Li for another 20 s. Data for CeO_2 and for mixed Zr–Ce oxide are shown in Fig. 14. The charge density for the intercalation was 14 mC cm^{-2} for the Zr–Ce oxide film and 26 mC cm^{-2} for the Ce oxide film. It is obvious that the films remain practically non-absorbing; the transmittance is changed by no more than a few percent.

4.2. *Special feature: analysis of opto–chronopotentiometry data*

Some insight into the peculiar absence of luminous absorptance under large charge insertion/extraction can be gleaned by combining optical transmittance data with chronopotentiometry. This latter technique gives more quantitative results than cyclic voltammetry.

In chronopotentiometry, the working electrode potential U_{Eq} is measured under slowly

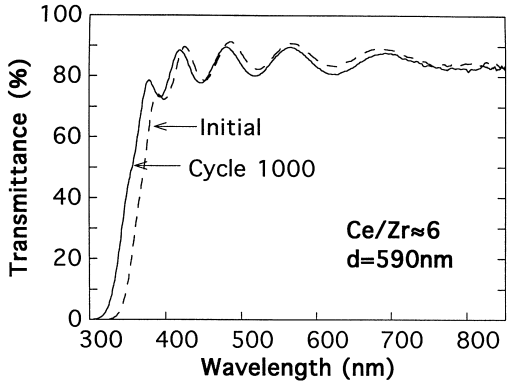

Fig. 13. Transmittance of an as-deposited and electrochemically cycled sputter-deposited Zr–Ce oxide film with the shown composition and thickness *d*.

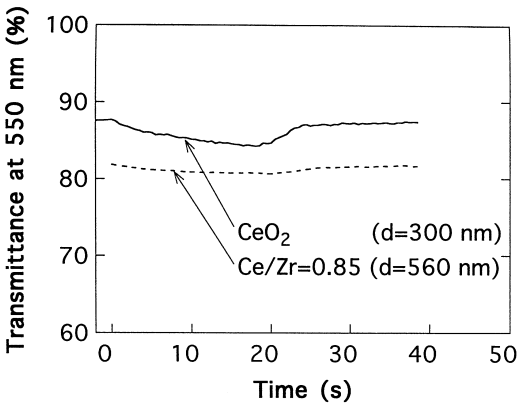

Fig. 14. Transmittance at $\lambda = 550$ nm during Li^+ intercalation in sputter-deposited films of Zr–Ce oxide and Ce oxide with the shown composition and thickness *d*. The potential was kept at 1.2 V versus Li during 20 s and was then changed to 4.5 V versus Li. Thickness differences and ensuing interference effects are responsible for the different overall levels of the transmittance.

increasing Li^+ content, so that it corresponds to (quasi) equilibrium conditions. Figure 15 reports results for ZrO_2, CeO_2 and Zr–Ce oxide, taken with galvanostatic charge insertion corresponding to a current of $\sim$1–10 μA cm^{-2}. The data are represented as $-dx/dU_{Eq}$ and $-dy/dU_{Eq}$ vs U_{Eq}, with x and y being the atomic ratios of Li/Zr and Li/Ce, respectively. The concomitant changes of the optical properties are illustrated by showing the transmittance at $\lambda = 550$ nm versus U_{Eq}.

We first consider the physical content of the chronopotentiometry experiment and observe that $-dx/dU_{Eq}$ (or $-dy/dU_{Eq}$) always carries information on the electron density of states since electrons, inserted along with the Li^+ ions to maintain charge neutrality, must enter empty electron states in the oxide. In most cases, $-dx/dU_{Eq}$ is related to the distribution of the ions over the available sites in the oxide, and when the ions begin to populate new types of sites there will be features introduced in the $-dx/dU_{Eq}$ vs U_{Eq} curves (West *et al.*, 1993; McKinnon, 1995). Furthermore, structural modifications upon ion intercalation may complicate the interpretation of the chronopotentiometry data.

Figure 15(a), pertaining to pure ZrO_2, shows a distinct peak in $-dx/dU_{Eq}$ at $U_{Eq} \approx 1.4$ V versus Li, and that the transmittance drops strongly for $U_{Eq} \approx 1.6$ V. In quantitative terms, an intercalation of $\sim$0.055 electrons per Zr atom—obtained by integrating the potentiometry curve—yields a drop of the transmittance by $\sim$20%. A corresponding coloration was not

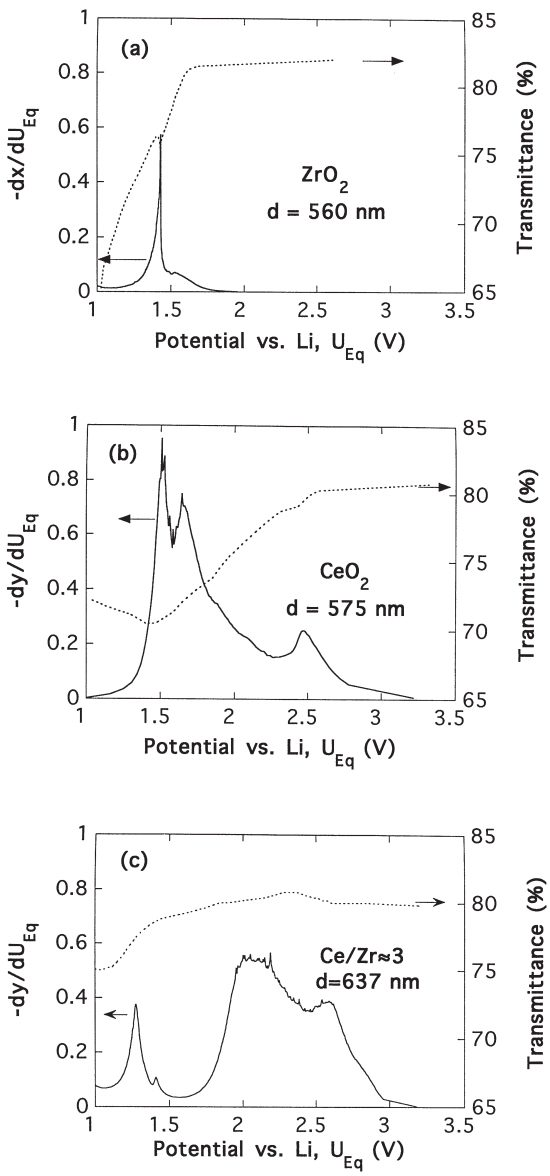

Fig. 15. Solid curves denote derivatives of x and y with respect to the working electrode potential U_{Eq}, where the number of intercalated Li^+ ions per Zr is denoted x for pure Zr dioxide (part a) and per Ce is denoted y for pure Ce oxide (part b) and for a mixed Zr–Ce oxide (part c). The *in situ* transmittance at $\lambda = 550$ nm, recorded during the chronopotentiometric measurements, is shown as dotted curves.

seen during the cyclic voltammetric measurements, this being a result of the film resistivity and the high potential sweep rate.

The lowering of the transmittance illustrated in Fig. 15(a) is consistent with literature data showing that (stabilized) zirconia becomes dark when exposed to high temperatures in a reducing atmosphere (Ingo, 1991; Nicoloso *et al.*, 1992) or by electroreduction (Nagle *et al.*, 1990; Pai Verneker and Nagle, 1990). A valency change from Zr^{4+} to Zr^{3+} has been recorded during the darkening (Ingo, 1991), and the absorption has been assigned to polaronic effects (He *et al.*, 1995). These notions are in agreement with a large amount of earlier work on cathodically coloring electrochromic oxides and, more specifically, with studies of colored Ti oxide (Granqvist, 1995). In analogy with the case of Ti oxide (Stashans *et al.*, 1996), we believe that the coloration of ZrO_2 is associated with electrons entering the Zr 4d states.

By integrating the chronopotentiometry data in Fig. 15(b) one obtains that ~ 0.5 Li^+ ions (and electrons) per Ce atom are intercalated in the studied potential regime. This value can be rationalized by contemplating that CeO_2 has 4f states in the bandgap that can host only one electron in the potential (i.e. energy) region used in this experiment; the 5d band as well as additional 4f states are located several eV above $4f^1$. Both energy band calculations (Koelling *et al.*, 1983) and analyses of photoabsorption and photoemission spectra (Wuilloud *et al.*, 1984; Kotani *et al.*, 1985, 1988) have led to the conclusion that the average number of 4f electrons in this material is 0.5. This means that an addition of 0.5 electrons per Ce atom is required to fill the Ce 4f states in the bandgap.

We now consider the most interesting film, viz. the Zr–Ce oxide film with a Ce/Zr ratio of 3 reported on in Fig. 15(c). An integration of the chronopotentiometry curve yields ~ 0.42 electrons per Ce atom between 3.2 and 1.6 V versus Li. The film is practically transparent at this potential, and the only effect of lowering the potential from 3.2 V versus Li is a slight anodic coloration by a few percent commencing at ~ 2.4 V. Going from 1.6 down to 1 V versus Li has a stronger influence on the transmittance, though, which drops from $\sim 80\%$ to $\sim 75\%$.

In order to give a tentative interpretation of these data for Zr–Ce oxide, one first observes that the $-\mathrm{d}y/\mathrm{d}U_{Eq}$ characteristic for pure CeO_2 is somewhat similar to the feature between 3.3 and 1.6 V versus Li for the mixed oxide film. The potential corresponding to an intercalation of ~ 0.5 electrons per Ce atom is ~ 1.3 V versus Li for CeO_2 (Fig. 15(b)) and ~ 1.6 V versus Li for mixed oxide (Fig. 15(c)). A displacement in this direction for the Zr–Ce oxide, relative to the case of pure CeO_2, is in line with our observations for Ti–Ce oxide films (Strømme Mattsson *et al.*, 1997), for which it was found that the Ce 4f states gradually shifted towards higher potentials (lower energies) with

decreasing Ce content. The Ti–Ce oxide did not change its color upon electron injection into the Ce 4f states, whereas this material colored cathodically at potentials low enough that Ti states started to host electrons. These facts lead us to propose that the charge balancing electrons, inserted along with Li^+ ion intercalation, initially occupy Ce 4f states, and that, once these states are fully populated, the excess electrons enter Zr 4d states and cause polaron absorption.

5. POLYMERIC PROTON-CONDUCTING ELECTROLYTES BASED ON ANTIMONIC ACID

The central part of an electrochromic five-layer device is the electrolyte or ion conductor (cf. Figure 1). It can be a thin (inorganic) film or a polymeric layer capable of H^+ or Li^+ transport. Many new systems are presently under development. Below we report on some progress related to a proton-conducting polymer electrolyte based on antimonic acid (Vaivars *et al.*, 1997).

We first note that amorphous antimonic acid in the form of a xerogel has been found to be a promising proton conductor compatible with oxide electrodes (Vaivars *et al.*, 1993) and that polymer electrolytes may be better suited for applications in electrochromic devices than powdered or xerogel-type electrolytes. Polymeric proton conductors—such as poly(ethylene oxide) or poly(vinyl alcohol) with strong acids (H_3PO_4, H_2SO_4) or ammonium salts—are under extensive investigation (Polak *et al.*, 1986; Donoso *et al.*, 1988; Petty-Weeks *et al.*, 1988; Scholmann *et al.*, 1992), but their high hygroscopicity and the poor chemical stability of electrode–electrolyte interfaces still pose practical problems. The present work considers composites of antimonic acid and aluminum oxide with poly(vinyl acetate) (PVA) and glycerin. Their low aggressivity and hygroscopicity make them interesting for applications.

The composite proton electrolyte was prepared as follows: an antimonic acid colloidal gel suspension in water (36 wt%) was made as described elsewhere by Vaivars *et al.* (1993). It was mixed with glycerin and a 50% suspension of PVA in water (proportions 1:0.35:0.32 by weight). This mixture was then dried to remove the water. The resulting composite was viscous and suitable for laminating devices. Depending on the preparation conditions, as discussed below, the electrolyte was transparent or light scattering. Partial substitution of the solid antimonic acid with inert, non-conductive oxides of aluminum (α-Al_2O_3) and silicon was investigated with the object of making the electrolyte less harmful.

Sample inspection by optical microscopy showed that the electrolyte consisted of two phases. One of these comprised agglomerated antimonic acid particles with diameters up to 1 μm; they cause strong light scattering. These particles were not in contact and cannot be responsible for electrical conductivity. By optimization of the synthesis conditions, it was possible to avoid agglomeration and hence to obtain a transparent electrolyte. The second part of the electrolyte was a homogeneous proton conducting phase. The grain size of the antimonic acid particles was 20 to 40 nm. XRD patterns of the films were identical to those of the well known pyrochlore structure of antimonic acid. This type of analysis also confirmed the nanometer-scale dimensions of the grains and showed that the aluminum oxide powder, suspended in the PVA–glycerin mixture, is hydrolyzed and amorphous.

Impedance spectrometry was carried out on electrolytes pressed between stainless steel electrodes, and conductivity data were obtained from Cole–Cole plots. The proton conductivity of the electrolyte is shown in Fig. 16; it is 10^{-4} S cm^{-1} at room temperature, and the activation energy is 0.21 ± 0.02 eV in the whole temperature stability range (-15 to $+60$°C). These properties are adequate for applications in electrochromic devices.

Figure 17 illustrates the influence of the water content on the conductivity for electrolytes with

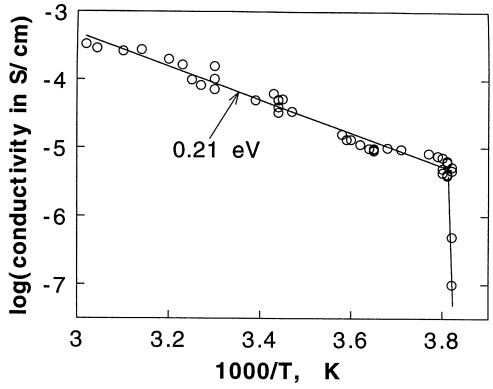

Fig. 16. Temperature (τ) dependence of the conductivity of an antimonic acid composite. The sloping line, fitted to the data points, gives the shown activation energy. The vertical line at $1000/\tau \approx 3.8$ signifies freezing.

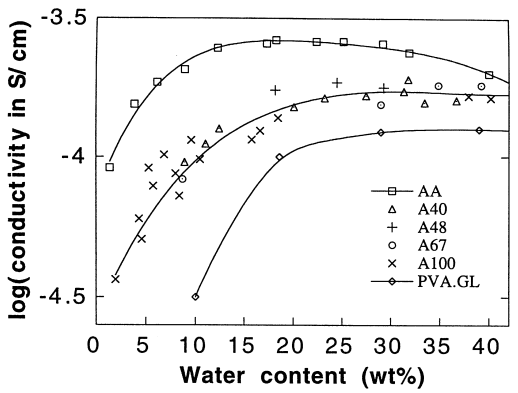

Fig. 17. Influence of water content on the conductivity of antimonic acid composite (AA), aluminum oxide composite (A100), poly(vinyl acetate) suspension in glycerine (PVA.GL) and antimonic acid–aluminum oxide mixed composites with the aluminum oxide content being 67% (A67), 48% (A48) and 40% (A40).

different compositions. The aluminum oxide content is characterized as a weight percentage of antimonic acid substituted with aluminum oxide (for example, the ratio aluminum oxide/antimonic oxide for the A67 sample is 67:33). It was possible to replace the antimonic acid with aluminum oxide without considerably decreasing the conductivity. The conductivity lay around 10^{-4} S cm^{-1} for all compositions up to pure aluminum oxide provided that the water content remained between 5 and 50 wt%. The conductivity of the PVA suspension in glycerin changed from 10^{-4} to 10^{-5} S cm^{-1} with the water concentration decreasing from 20 to 5 wt%. However, the proton conductivity of the composites showed a weaker dependence on the water content. For composites containing only antimonic acid or aluminum oxide, the conductivity was above 10^{-5} S cm^{-1} down to 1 wt% of water.

The electrolyte was tested in laminated electrochromic devices, with W oxide and Ir oxide (or mixed Ti–Ce oxide) serving as the optically active layer and the counter electrode, respectively. Plastic spacers were used to ensure a uniform thickness of the electrolyte (60 to 120 μm). The laminated devices were sealed with epoxy resin.

The electrochromic layers were observed to corrode after 10^4 to 10^5 color/bleach cycles. The chemical corrosion of the devices is at least partly due to water absorbed in the proton electrolyte. The estimated optimal content of water for the antimonic acid composite electrolyte corresponded to the hydrate $Sb_2O_5 \cdot 3H_2O$ (1 wt% of water in Fig. 17). For this composition, the conductivity is higher than 10^{-5} S cm^{-1}, which may be a minimum for applications in electrochromic devices, and all of the water is strongly bonded and therefore not chemically corrosive. A considerable decrease in conductivity was observed when the amount of hydrate water in the antimonic acid was reduced.

Preliminary results show that the device lifetime was slightly improved by use of electrolytes containing aluminum oxide. The addition of silicon oxide lowered the conductivity, so that it lay close to that of the pure PVA–glycerin mixture, but allowed the temperature stability region to be extended to above 100°C.

6. CONCLUSION AND REMARKS

A very large number of electrochromic device designs have been proposed during the past several years as reviewed by Granqvist (1993a, 1995) and others. The object here is not to attempt any survey of these. Only one example of an as yet unpublished device is given; it includes a sputter-deposited W oxide film (prepared according to Section 3.2), a Zr–Ce oxide counter electrode (as described in Section 4), a Li^+ conducting polymer electrolyte laminate (Azens *et al.*, 1992) and transparent electrically conducting ITO layers.

Figure 18(a) displays the spectral transmittance through the full five-layer stack interposed between glass substrates and mounted in the sample compartment of a spectrophotometer. Different states of coloration were obtained by applying a voltage between the transparent electrical conductors. The dash-dotted curve shows data for the fully bleached sample. The transmittance is in the 70 to 80% range over the full luminous spectrum. Coloration to increasingly low transmittance was accomplished by application of a voltage U_{col} in the 3.2 to 3.5 V interval. The dynamics of the coloration/bleaching of a 2.5×2.5 cm^2 sample is illustrated in Fig. 18(b). Coloration takes place during the course of a few minutes, whereas bleaching is somewhat faster.

As a final note we stress that research and development of electrochromic devices have progressed at a steady pace for several years, and the first products based on this phenomenon exist on the market. Electrochromic glazings for buildings are not yet available in consumer products, but it has recently been reported that the market introduction of such

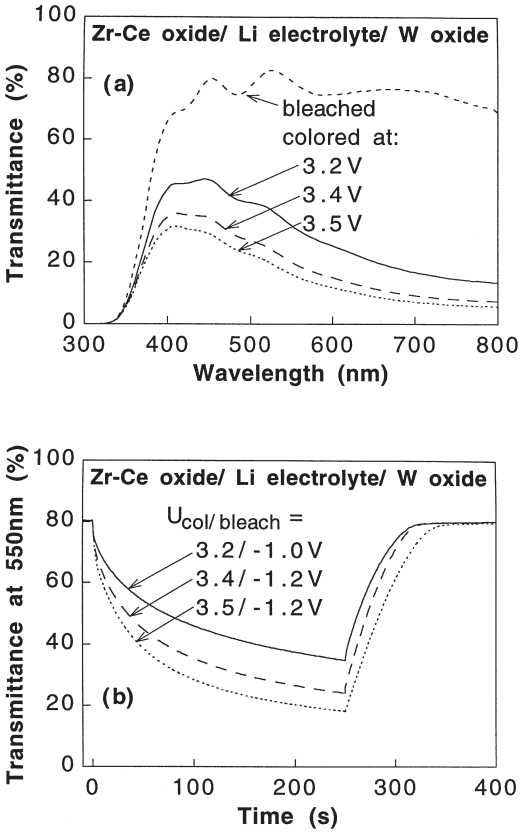

Fig. 18. Spectral transmittance (part a) and time-dependent transmittance (part b) in the mid-visible for a device including electrochromic W oxide, a Zr–Ce counter electrode and a polymeric Li^+ conducting electrolyte. Coloring and bleaching were accomplished by application of the shown voltages U_{col} and U_{bleach}, respectively.

glazings is imminent. They are of much interest within the architectural (and automotive) sectors, and—as shown in this review paper—they can produce windows going from an almost completely transparent state to one with a low transmittance, thus enabling the solar energy throughput to be varied for energy purposes and the luminous throughput to be varied for lighting purposes.

REFERENCES

Agnihotry S. A. and Chandra S. (1994) Electrochromic devices: present and forthcoming technology. *Indian J. Eng. Mater. Sci* **1,** 320–334.

Amra C. (1993) First-order vector theory of bulk scattering in optical multilayers. *J. Opt. Soc. Am. A* **10,** 365–374.

Andersson A. M., Granqvist C. G. and Stevens J. R. (1989) An electrochromic Li_xWO_3/polymer electrolyte/$Li_yV_2O_5$ device: towards an all-solid-state smart window. *Appl. Opt* **28,** 3295–3302.

Ashrit P. V., Benaissa K., Bader G., Girouard F. E. and Truong V.-V. (1993) Lithiation studies on some transition metal oxides for an all-solid thin film electrochromic system. *Solid State Ionics* **59,** 47–57.

Azens A., Granqvist C. G., Pentjuss E., Gabrusenoks J. and Barczynska J. (1995) Electrochromism of fluorinated and electron bombarded tungsten oxide films. *J. Appl. Phys* **78,** 1968–1974.

Azens A., Kullman L., Ragan D. D., Granqvist C. G., Hjörvarsson B. and Vaivars G. (1996) Optical and electrochemical properties of dc magnetron sputtered Ti–Ce oxide films. *Appl. Phys. Lett* **68,** 3701–3703.

Azens A., Talledo A., Andersson A. M., Niklasson G. A., Stjerna B., Granqvist C. G. and Stevens J. R. (1992) W oxide/polymer laminate/V oxide electrochromic smart windows: recent advances. *Proc. Soc. Photo-Opt. Instrum. Eng* **1728,** 103–117.

Bange K., Gambke T. and Sparschuh G. (1995) Optically active thin film coatings, In *Handbook of Optical Properties*, Vol. 1, Hummel R. E. and Guenther K. H. (Eds), pp. 105–134. CRC Press, Boca Raton.

Baudry P., Aegerter M. A., Deroo D. and Valla B. (1991) Electrochromic window with lithium conductive polymer electrolyte. *J. Electrochem. Soc* **138,** 460–465.

Camino D., Deroo D., Salardenne J. and Treuil N. (1995) $(CeO_2)_x$–$(TiO_2)_{1-x}$: counter electrode materials for lithium electrochromic devices. *Solar Energy Mater. Solar Cells* **39,** 349–366.

Carniglia C. K. (1979) Scalar scattering theory for multilayer optical coatings. *Opt. Eng* **18,** 104–115.

Cava R. J., Phillips J. M., Kwo L., Thomas G. A., van Dover R. B., Carter S. A., Krajewski J. J., Peck W. F., Marshall, Jr J. H. and Rapkine D. H. (1994) $GaInO_3$: a new transparent conducting oxide. *Appl. Phys. Lett* **64,** 2071–2072.

Cogan S. F., Anderson E. J., Plante T. D. and Rauh R. D. (1985) Materials and devices in electrochromic window development. *Proc. Soc. Photo-Opt. Instrum. Eng* **562,** 23–31.

Cogan S. F., Rauh R. D., Nguyen N. M., Plante T. D. and Westwood J. D. (1993) Electrochromism in Nb–V and Cr–V mixed oxides. *J. Electrochem. Soc* **140,** 112–115.

Deb S. K. (1992) Opportunities and challenges of electrochromic phenomena in transition metal oxides. *Solar Energy Mater. Solar Cells* **25,** 327–338.

Deb S. K. (1995) Reminiscences on the discovery of electrochromic phenomena in transition metal oxides. *Solar Energy Mater. Solar Cells* **39,** 191–201.

Deb S. K. and Witzke H. (1975) The solid state electrochromic phenomenon and its applications to display devices, In *Proc. Int. Electron Devices Meeting*, Washington, pp. 393–397. IEEE, New York.

Donoso P., Gorecki W., Berthier C., Defendini F., Poinsignon C. and Armand M. (1988) NMR, conductivity and neutron scattering investigation of ionic dynamics in the anhydrous polymer protonic conductor $PEO(H_3PO_4)_x$. *Solid State Ionics* **28–30,** 969–974.

Duparré A. (1995) Light scattering of thin dielectric films, In *Handbook of Optical Properties*, Vol. 1, Hummel R. E. and Guenther K. H. (Eds), pp. 273–303. CRC Press, Boca Raton.

Enoki H., Nakayama T. and Echigoya J. (1992) The electrical and optical properties of the ZnO–SnO_2 thin films prepared by RF magnetron sputtering. *Phys. Status Solidi B* **129,** 181–191.

Goldner R. B., Arntz F. O. and Haas T. E. (1994) d-Electrons and two active thin film devices for achieving a solar energy economy. *Solar Energy Mater. Solar Cells* **32,** 421–428.

Gomes M. A. B., Goncalves D., Pereira de Souza E. C., Valla B., Aegerter M. A. and Bulhões L. O. S. (1992) Solid state electrochromic display based on polymer electrode – polymer electrolyte interface. *Electrochim. Acta* **37,** 1653–1656.

Granqvist C. G. (1993a) Electrochromic tungsten-oxide-based thin films: physics, chemistry, and technology, In *Physics of Thin Films*, Vol. 17, Francombe M. H. and Vossen J. L. (Eds), pp. 301–370. Academic, San Diego.

Granqvist C. G. (1993b) Transparent conductive electrodes for electrochromic devices. *Appl. Phys. A* **57,** 19–24.

Granqvist C. G. (1995) *Handbook of Inorganic Electrochromic Materials*, pp. 1–633. Elsevier, Amsterdam.

Granqvist C. G. (1997) Electrochromism and electrochromic devices, In *CRC Handbook of Solid State Electrochemistry*, Gellings P. G. and Bouwmeester H. J. M. (Eds), pp. 587–615. CRC Press, Boca Raton.

Gutarra A., Azens A., Stjerna B. and Granqvist C. G. (1994) Electrochromism of sputtered fluorinated titanium oxide thin films. *Appl. Phys. Lett* **64,** 1604–1606.

Hamberg I. and Granqvist C. G. (1986) Evaporated Sn-doped In_2O_3 films: basic optical properties and applications to energy efficient windows. *J. Appl. Phys* **60,** R123–R159.

He T., Becker K. D. and Tannhauser D. S. (1995) An optical in-situ study of the re-oxidation kinetics of calcia-stabilized zirconia. *Ber. Bunsenges. Phys. Chem* **99,** 658–666.

Hjelm A., Granqvist C. G. and Wills J. M. (1996) Electronic structure and optical properties of WO_3, $LiWO_3$, $NaWO_3$, and HWO_3. *Phys.* Rev. B **54,** 2436–2445.

Ho K.-C., Rukavina T. G. and Greenberg C. B. (1994) Tungsten oxide – Prussian Blue electrochromic system based on a proton-conducting polymer electrolyte. *J. Electrochem. Soc* **141,** 2061–2067.

Inaba H., Iwaku M., Nakase K., Yasukawa H., Seo I. and Oyama N. (1995) Electrochromic display device of tungsten trioxide and Prussian Blue films using polymer gel electrolyte of methacrylate. *Electrochim. Acta* **40,** 227–232.

Ingo G. M. (1991) Origin of darkening in 8 wt% yttria–zirconia plasma-sprayed thermal barrier coatings. *J. Am. Ceram. Soc* **74,** 381–386.

Johnson P. C. (1991) The cathodic arc plasma deposition of thin films, In *Thin Film Processes*, Vol. 2, Vossen J. L. and Kern W. (Eds), pp. 209–280. Academic, San Diego.

Kamimori T., Nagai J. and Mizuhashi M. (1987) Electrochromic devices for transmissive and reflective light control. *Solar Energy Mater* **16,** 27–38.

Kéomany K., Petit J.-P. and Deroo D. (1995) Electrochemical insertion in sol–gel made CeO_2–TiO_2 from lithium conducting polymer electrolyte: relation with the material structure. *Solar Energy Mater. Solar Cells* **36,** 397–408.

Kéomany K., Poinsignon C. and Deroo D. (1994) Sol gel preparation of mixed cerium–titanium oxide thin films. *Solar Energy Mater. Solar Cells* **33,** 429–441.

Kharrazi M., Azens A., Kullman L. and Granqvist C. G. (1997) High-rate dual-target d.c. magnetron sputter deposition of electrochromic MoO_3 films. *Thin Solid Films* **295,** 117–121.

Kim D.-J., Lattice parameters, ionic conductivities, and solubility limits in fluorite-structure MO_2 oxide ($M = Hf^{4+}$, Zr^{4+}, Ce^{4+}, Th^{4+}, U^{4+}) solid solutions. *J. Am. Ceram. Soc* **72,** (1989) 1415–1421.

Koelling D. D., Boring A. M. and Wood J. H. (1983) The electronic structure of CeO_2 and PrO_2. *Solid State Commun* **47,** 227–232.

Kotani A., Jo T. and Parlebas J. C. (1988) Many-body effects in core-level spectroscopy of rare-earth compounds. *Adv. Phys* **37,** 37–85.

Kotani A., Mizuta H., Jo T. and Parlebas J. C. (1985) Theory of core photoemission spectra in CeO_2. *Solid State Commun* **53,** 805–810.

Kullman L., Azens A. and Granqvist C. G. (1997) Decreased electrochromism in Li-intercalated Ti oxide films containing La, Ce, and Pr. *J. Appl. Phys* **81,** 8002–8010.

Kullman L., Rönnow D. and Granqvist C. G. (1996a) Elastic light scattering and electrochemical durability of electrochromic tungsten-oxide-based films. *Thin Solid Films* **288,** 330–333.

Kullman L., Veszelei M., Ragan D. D., Isidorsson J., Vaivars G., Kanders U., Azens A., Schelle S., Hjörvarsson B. and Granqvist C. G. (1996b) Cerium-containing counter electrodes for transparent electrochromic devices. *Proc. Soc. Photo-Opt. Instrum. Eng* **2968,** 219–224.

Lampert C. M. (1998) Smart switchable glazing for solar energy and daylight control. *Solar Energy Mater. Solar Cells* **52,** 207–221.

Lampert C. M. and Granqvist C. G. (Eds) (1990) *Large-Area Chromogenics: Materials and Devices for Transmittance Control*, pp. 2–606. SPIE Opt. Eng. Press, Bellingham.

Lampert C. M., Visco S. J., Doeff M. M., Ma Y. P., He Y. and Giron J.-C. (1994) Characteristics of laminated electrochromic devices using polyorganic–disulfide electrodes. *Solar Energy Mater. Solar Cells* **33,** 91–105.

Lavrencic Stangar U., Orel B., Grabec I., Ogorevc B. and Kalcher K. (1993) Optical and electrochemical properties of CeO_2 and CeO_2–TiO_2 coatings. *Solar Energy Mater. Solar Cells* **31,** 171–185.

Lindström T., Kullman L., Rönnow D., Ribbing C.-G. and Granqvist C. G. (1997) Electrochromic control of thin film light scattering. *J. Appl. Phys* **81,** 1464–1469.

McKinnon W. R. (1995) Insertion electrodes I: atomic and electronic structure of the hosts and their insertion compounds, In *Solid State Electrochemistry*, Bruce P. G. (Ed), pp. 163–198. Cambridge University Press, Cambridge.

Minami T., Kakumu T. and Takata S. (1996a) Preparation of transparent and conductive In_2O_3–ZnO films by radio frequency magnetron sputtering. *J. Vac. Sci. Technol. A* **14,** 1704–1708.

Minami T., Kakumu T., Takeda Y. and Takata S. (1996b) Highly transparent and conductive ZnO–In_2O_3 thin films prepared by d.c. magnetron sputtering. *Thin Solid Films* **290–291,** 1–5.

Minami T., Sonohara H., Kakumu T. and Takata S. (1995a) Highly transparent and conductive $Zn_2In_2O_5$ thin films prepared by RF magnetron sputtering. *Jpn. J. Appl. Phys* **34,** L971–L974.

Minami T., Sonohara H., Takata S. and Sato H. (1994) Highly transparent and conductive zinc-stannate thin films prepared by RF magnetron sputtering. *Jpn. J. Appl. Phys* **33,** L1693–L1696.

Minami T., Takata S., Sato H. and Sonohara H. (1995b) Properties of transparent zinc-stannate conducting films prepared by radio frequency magnetron sputtering. *J. Vac. Sci. Technol. A* **13,** 1095–1099.

Mochizuki S. (1982) Infrared optical properties of cerium dioxide. *Phys. Status Solidi B* **114,** 189–199.

Monk P. M. S., Mortimer R. J. and Rosseinsky D. R. (1995) *Electrochromism: Fundamentals and Applications*, pp. 1–216. VCH, Weinheim.

Nagle D., Pai Verneker V. R., Petelin A. N. and Groff G. (1990) Optical absorption of electrolytically colored single crystals of yttria-stabilized zirconia. *Mater. Res. Bull* **24,** 619–623.

Nicoloso N., Löbert A. and Leibold B. (1992) Optical absorption studies of tetragonal and cubic thin-film yttria-stabilized zirconia. *Sensors and Actuators B* **8,** 253–256.

Pai Verneker V. R. and Nagle D. (1990) Effect of reduction on Vickers hardness of stabilized zirconia. *J. Mater. Sci. Lett* **9,** 192–194.

Petty-Weeks S., Zupancic J. J. and Swedo J. R. (1988) Proton conducting interpenetrating polymer networks. *Solid State Ionics* **31,** 117–125.

Phillips J. M., Kwo J., Thomas G. A., Carter S. A., Cava R. J., Hou S. Y., Krajewski J. J., Marshall J. H., Peck W. F., Rapkine D. H. and van Dover R. B. (1994) Transparent conducting thin films of $GaInO_3$. *Appl. Phys. Lett* **65,** 115–117.

Polak A., Petty-Weeks S. and Beuhler A. J. (1986) Applications of novel proton-conducting polymers to hydrogen sensing. *Sensors and Actuators* **9,** 1–7.

Rauh D. (1995) Design and fabrication of electrochromic light modulators. *Solar Energy Mater. Solar Cells* **39,** 145–154.

Rönnow D. and Veszelei E. (1994) Design review of an instrument for spectroscopic total integrated light scattering measurements in the visible wavelength region. *Rev. Sci. Instrum* **65,** 327–334.

Rönnow D., Kullman L. and Granqvist C. G. (1996) Spectroscopic light scattering from electrochromic tungsten-oxide-based films. *J. Appl. Phys* **80,** 423–430.

Scholmann D., Trinquet O. and Lassegues J. C. (1992) Properties and application of a proton conducting polymer: the BPEI, x H_3PO_4 system. *Electrochim. Acta* **37,** 1619–1621.

Shen P., Huang H. and Tseung A. C. C. (1992) Improvements in the life of WO_3 electrochromic films. *J. Mater. Chem* **2,** 497–499.

Shigesato Y., Hayashi Y., Masui A. and Haranou T. (1991) The structural changes of indium–tin oxide and a-WO_3 films by introducing water to the deposition process. *Jpn. J. Appl. Phys* **30,** 814–819.

Stashans A., Lunell S., Bergström R. and Lindquist S.-E. (1996) Theoretical study of lithium intercalation in rutile and anatase. *Phys. Rev. B* **53,** 159–170.

Steele B. C. H. and Golden S. J. (1991) Variable transmission electrochromic windows utilizing tin-doped indium oxide counterelectrodes. *Appl. Phys. Lett* **59,** 2357–2359.

Strømme Mattsson M., Azens A., Niklasson G. A., Granqvist C. G. and Purans J. (1997) Li intercalation in Ti–Ce oxide films: energetics and ion dynamics. *J. Appl. Phys* **81,** 6432–6437.

Svensson J. S. E. M. and Granqvist C. G. (1985) Electrochromic coatings for "smart windows". *Solar Energy Mater* **12,** 391–402.

Svensson J. S. E. M. and Granqvist C. G. (1986) Electrochromic hydrated nickel oxide coatings for energy efficient windows: optical properties and coloration mechanism. *Appl. Phys. Lett* **49,** 1566–1568.

Svensson J. S. E. M. and Granqvist C. G. (1987) Optical properties of electrochromic hydrated nickel oxide coatings made by rf sputtering. *Appl. Opt* **26,** 1554–1556.

Talledo A. and Granqvist C. G. (1995) Electrochromic vanadium-oxide based films: structural, electrochemical, and optical properties. *J. Appl. Phys* **77,** 4655–4666.

Talledo A., Stjerna B. and Granqvist C. G. (1994) Optical properties of lithium-intercalated V_2O_5-based films treated in CF_4 gas. *Appl. Phys. Lett* **65,** 2774–2776.

Tassi E. L. and de Paoli M.-A. (1994) An electrochromic device based on association of the graft copolymer of polyaniline and nitric rubber with WO_3. *Electrochim. Acta* **39,** 2481–2484.

Taylor T. A. and Patterson H. H. (1994) Spectroscopic properties of WO_3 thin films: polarized FT-IR/ATR, X-ray diffraction, and electronic absorption. *Appl. Spectrosc* **48,** 674–677.

Ueda N., Omata T., Hikuma N., Ueda K., Mizoguchi H., Hashimoto T. and Kawazoe H. (1992) New oxide phase with wide band gap and high electroconductivity, $MgIn_2O_4$. *Appl. Phys. Lett* **61,** 1954–1955.

Un'no H., Hikuma N., Omata T., Ueda N., Hashimoto T. and Kawazoe H. (1993) Preparation of $MgIn_2O_{4-x}$ thin films on glass substrate by RF sputtering. *Jpn. J. Appl. Phys* **32,** L1260–L1262.

Vaivars G., Kleperis J., Azens A., Granqvist C. G. and Lusis A. (1997) Proton conducting composite electrolytes based on antimonic acid. *Solid State Ionics* **97,** 365–368.

Vaivars G., Kleperis J. and Lusis A. (1993) Antimonic acid hydrate xerogels as proton electrolytes. *Solid State Ionics* **61,** 317–321.

Veszelei M., Kullman L., Azens A., Granqvist C. G. and Hjörvarsson B. (1997) Transparent ion intercalation films of Zr–Ce oxide. *J. Appl. Phys* **81,** 2024–2026.

Veszelei M., Kullman L., Strømme Mattsson M., Azens A. and Granqvist C. G. (1998) Optical and electrochemical properties of Li^+ intercalated Zr–Ce oxide and Hf–Ce oxide films. *J. Appl. Phys* **83,** 1670–1676.

West K., Zachau-Christiansen B., Jacobsen T. and Skaarup S. (1993) Lithium intercalation in oxides: EMF related to structure and chemistry, In *Solid State Ionics III*, Nazri G.-A., Tarascon J.-M. and Armand M. (Eds), 9.47–9.55. Materials Research Society, Pittsburgh.

Wuilloud E., Delley B., Schneider W.-D. and Baer Y. (1984) Spectroscopic evidence for localized and extended *f*-symmetry states in CeO_2. *Phys. Rev. Lett* **53,** 202–205.

Yamanaka K. (1991) The electrochromic behavior of anodically electrodeposited iridium oxide films and the reliability of transmittance variable cells. *Jpn. J. Appl. Phys* **30,** 1285–1289.

Zhang J.-G., Benson D. K., Tracy E., Deb S. K., Czanderna A. W. and Crandall R. S. (1994) Optimization study of solid-state-electrochromic devices based on WO_3/lithium-polymer electrolyte/V_2O_5 structures. *J. Electrochem. Soc* **141,** 2795–2800.